International Journal of Low-Carbon Technologies Advance Access published November 23, 2011

Study of zinc hydroxy acetate as catalyst in the esterification reaction of fatty acids

Deborath M. Reinoso[1], María B. Fernandez[2], Daniel E. Damiani[1] and Gabriela M. Tonetto[1*]

[1]Planta Piloto de Ingeniería Química, PLAPIQUI (UNS – CONICET), Camino 'La Carrindanga' Km 7, CC 717, Bahía Blanca CP 8000, Argentina; [2]Grupo TECSE, Facultad de Ingeniería, Universidad Nacional del Centro de la Provincia de Buenos Aires, Olavarría, Argentina

Abstract

In this work, the esterification of oleic acid (OA) with methanol (MOH) using layered heterogeneous catalysts under various reaction conditions to produce biodiesel was studied. The zinc hydroxy nitrate salt $Zn_5(OH)_8(NO_3)_2 \cdot 2H_2O$ (abbreviated Zn-N) and zinc hydroxy acetate $Zn_5(OH)_8(CH_3COO)_2 \cdot 4H_2O$ (abbreviated Zn-A), which have a layered structure, were synthesized (chemical precipitation) and characterized. Tests for the selection of reaction conditions that maximize the yield to methyl esters were performed. The variables considered were temperature, OA:MOH molar ratio and catalyst loading, selecting the study intervals within the range of feasible operating conditions for the catalysts. The layered solid Zn-A was seen to be more active than Zn-N for the esterification of OA. When working at 140°C, 1:30 OA:MOH molar ratio and catalyst loading of 3% w/w, conversions of 87.0 and 73.4% were obtained for Zn-A and Zn-N, respectively.

Keywords: esterification; zinc hydroxy acetate; zinc hydroxy nitrate; oleic acid

*Corresponding author: gtonetto@plapiqui.edu.ar

Received 9 August 2011; revised 6 October 2011; accepted 18 October 2011

1 INTRODUCTION

The synthesis of biodiesel (FAME, fatty acid methyl esters) from renewable biological sources, including animal fats and vegetable oils, has received considerable attention due to its environmental advantages and sustainable production in comparison with fossil fuels [1]. Biodiesel can completely or partially replace diesel fuel produced from petroleum; it is ecological, biodegradable, nontoxic and it presents an emissions profile sufficiently low as to reduce the greenhouse effect and meet the requirements of the Kyoto protocol.

In general, biodiesel is produced by transesterification of vegetable oils with methanol (MOH) in the presence of a base catalyst (NaOH, KOH and sodium methoxide) [2]. This type of process has the disadvantage of requiring refined vegetable oil with a water content of $<$500 ppm water and with free fatty acid (FFA) concentrations lower than 2–5% [3, 4]. This limit depends on the type of technology being used in the production of biodiesel. In large-scale industrial continuous plants, the acidity of the raw material is specified as lower than 0.1%. In small-scale discontinuous plants, values of 3 or 4% are perfectly acceptable.

In order to use acid raw materials (waste vegetable oil, tallow, lard, yellow grease or chicken fat), which present a high FFA content and therefore have a low cost, in the production of biodiesel, it is first necessary to remove that acidity, and this is possible by an acid esterification stage prior to the conventional transesterification [5].

The study of the application of heterogeneous catalysts that lead to more efficient processes is considered of great importance and utility, even more if they are capable of catalyzing both reactions: the esterification of fatty acids and the transesterification of triglycerides. Some of the advantages of using a heterogeneous catalyst over a homogeneous one are: reuse of the catalyst, implementation of continuous processes, use of raw materials of various sources, no soap is formed, simpler purification, no neutralization step is necessary. Among the disadvantages, there is the possibility of mass-transfer resistances, higher reaction temperature and possible leaching of the active species [6].

Esterification and transesterification reactions using heterogeneous catalysts based on layered double hydroxides (LDH) have been proposed in a series of recent publications [7, 8]. Layered hydroxy salts containing interchangeable anions are a

doi:10.1093/ijlct/ctr040

family of inorganic solids that are receiving increasing attention. Zinc hydroxy nitrate ($Zn_5(OH)_8(NO_3)_2 \cdot 2H_2O$) exhibits a very good activity in esterification and transesterification reactions [9, 10]. However, it was also reported that during esterification of lauric acid, the layered solid gradually decomposes and loses its structure, maintaining its catalytic activity [9]. It was also found that when the salt is treated at temperatures above 140°C, it starts to decompose, and its activity in transesterification in subsequent reuses begins to decrease [11].

The structure of hydroxy salts is given by the general formula $M^{2+}(OH)_{2-X}(A^{n-})_{X/n}yH_2O$, where the bivalent metal ion M^{2+} and the anion A^{n-} have many possible variations. Zinc hydroxy nitrate presents a layered structure consisting of infinite brucite-like layers, where one-quarter of the octahedrally coordinated Zn atom sites are vacant, and on either side of the empty octahedra there are zinc atoms tetrahedrally coordinated to OH groups (forming the base of the tetrahedra) with a water molecule occupying the apex. The nitrate groups are located between the sheets, and they are not involved in the coordination of the Zn atoms [12].

Zinc hydroxy acetate $Zn_5(OH)_8(CH_3CO_2)_2 \cdot 4H_2O$ presents the advantage of a better thermal stability. The mode of interaction between the acetate anion and the matrix cation is not yet clear. Poul *et al.* [13] and Hosono *et al.* [14] proposed that the anion occurs as a free species, while in a recent report, Kandare and Hossenlopp [15] proposed (on the basis of FTIR data) that the acetate anion is directly coordinated to the matrix cation as a unidentate ligand via $M-OCOCH_3$ bonds.

Taking into account the potential use of Zn-based catalysts for biodiesel production, the present work studies the activity of zinc hydroxy acetate and zinc hydroxy nitrate in the esterification of oleic acid (OA) with MOH. The effects of the reaction parameters (reaction temperature, catalyst concentration and MOH/OA molar ratio) were analyzed in order to determine the experimental conditions that maximize the formation of methyl oleate.

2 EXPERIMENTAL

2.1 Catalyst preparation

The synthesis of $Zn_5(OH)_8(NO_3)_2 \cdot 2H_2O$ (Zn-N) was carried out according to the procedure reported by Newman and Jones [16]. The Zn-N salt was prepared by drop wise addition of 50 cm^3 of 0.75 M sodium hydroxide solution to 20 cm^3 of a 3.5 M aqueous zinc nitrate solution at room temperature, with constant stirring. The precipitate obtained was filtered, washed with deionized water and dried for 12 h at 50°C.

The synthesis of $Zn_5(OH)_8(CH_3CO_2)_2 \cdot 4H_2O$ (Zn-A) with idealized composition was carried out by the titration method according to Biswick *et al.* [17] with modifications. The Zn-A salt was prepared by drop wise addition of 50 cm^3 of 0.75 M sodium hydroxide solution to 100 cm^3 of a 0.7 M aqueous zinc acetate dehydrate aqueous solution at room temperature, with constant stirring. The precipitate obtained was filtered, washed with deionized water and dried for 12 h at 50°C.

2.2 Catalyst characterization

The structure of Zn-A and Zn-N catalysts (synthesized and recovered after reaction) was identified and studied by X-ray diffraction (Philips PW1710, using Cu-Kα radiation scan in the 2θ range of 5–70°) and by diffuse-reflectance Fourier transform-infrared spectroscopic (DRIFTS, Nicolet 6700FT-IR spectrometer).

The specific surface area of the solids was obtained from the N_2 adsorption isotherm at 77 K by the BET method, using a Nova 1200e Quantachrome instrument, and the pore size distribution was calculated by the BJH method. The morphology and particle size distribution of the powder catalysts was analyzed by SEM using a JEOL 35 CF scanning electron microscope.

2.3 Catalytic tests

The esterification tests were carried out in a 600 cm^3 Parr reactor (internal diameter: 64 mm) operated in batch mode, with an agitation rate of 500 rpm, equipped with a 4-angled blade stirrer. The reactants used were OA (Anedra) and MOH (Anedra HPLC quality). Total reaction time was 2 h. Tests with different agitation rates were also performed in order to find the optimal reaction rate.

A certain amount of sample was dissolved in ethanol and sulphuric ether (50:50%v/v) in order to determine by titration the remaining amount of OA (according to UNE-EN 14104 norm). A 0.02 N KOH ethanol solution was used for titration. Acidity was calculated by:

$$a = \frac{V \cdot M_{KOH} \cdot C}{W} \quad (1)$$

where a = acidity index (mg KOH/g sample), C = solution concentration KOH (mol/l), W = weight of the sample (g), M_{KOH} = molecular weight of KOH (g/mol), V = volume of the solution used in titration (ml).

2.4 Experimental design

At first, a 2^3 design with two repetitions in the central point was made to study the experimental conditions in the proposed levels (Tables 1 and 2), and thus 10 different tests were planned and carried out randomly in order to maintain the

Table 1. *Values of the variables used in the study.*

Parameter	Level		
	−1	0	1
Temperature (°C)	100	120	140
Catalyst loading (% wt with respect to OA)	1	2	3
MOH:OA molar ratio (mol:mol)	10	20	30

Table 2. *2^3 factorial design with two repetitions in the central point.*

Temperature (A)	Catalyst loading (B)	MOH:OA molar ratio (C)
−1	1	1
−1	−1	1
−1	1	−1
−1	−1	−1
0	0	0
0	0	0
1	1	1
1	−1	−1
1	−1	1
1	1	−1

Table 3. *Face-centered CCD with two repetitions of the central point.*

Temperature (A)	Catalyst loading (B)	MOH:OA molar ratio (C)
−1	1	1
−1	−1	1
−1	1	−1
−1	−1	−1
0	0	0
0	0	0
1	1	1
1	−1	−1
1	1	−1
1	−1	1
−1	0	0
1	0	0
0	−1	0
0	1	0
0	0	−1
0	0	1

independence of the unknown and uncontrolled factors that could affect the results. For the selection of the levels, it was taken into account that the esterification reaction is reversible, and thus it is convenient to use an excess of MOH, in order to shift the equilibrium towards products, and that the catalyst decomposes above 140°C, being then preferable to work with low catalyst loadings.

The natural variables were coded according to Equation (2)

$$X_{\text{coded}} = \frac{2X - X_{\max} - X_{\min}}{X_{\max} - X_{\min}} \qquad (2)$$

where X, $X_{\max}$ and $X_{\min}$ are the actual, maximum and minimum value, respectively, of the natural variables (temperature, catalyst loading and MOH:OA molar ratio) in their original units (°C, % p/p, mol/mol). X_{coded} is the coded value of the variable (A, B and C being temperature, catalyst loading and molar ratio, respectively).

Later, the 2^3 design was extended to a central composite design (CCD), with $\alpha = 1$, face-centered (Table 3). Even though this design is non-rotatable, it was decided to select $\alpha = 1$ and not higher due to the physical restrictions generated by extending the conditions of the studied variables. As indicated above, it is not possible to operate at temperatures above 140°C because the catalyst decomposes. On the other hand, it is not possible to increase the catalyst concentration without increasing the MOH:OA ratio, since it becomes more difficult to take samples because the catalyst suffers a change in its layered structure.

The conversion of OA for a reaction time of 2 h was selected as the response variable for this study. The response surface plots and the statistical analysis for each response were performed using Statgraphic Centurion®.

Table 4. *Morphological properties of the synthesized solids.*

Properties	Catalysts	
	Zn-N	Zn-A
Specific surface area (m^2/g)	28	25
Pore volume (cm^3/g)	5.1×10^{-2}	5.4×10^{-2}
Pore radius (nm)	23	23

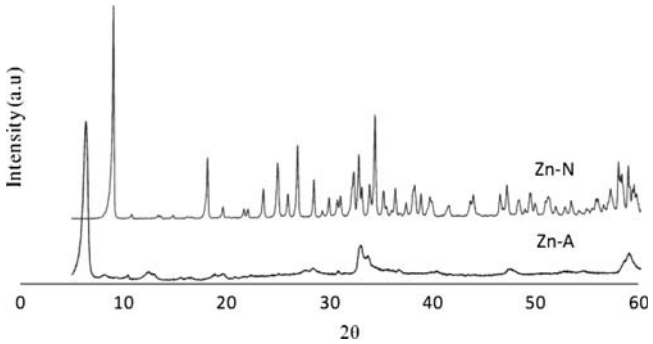

Figure 1. *DRX spectra for Zn-N and Zn-A.*

3 RESULTS AND DISCUSSION

3.1 Catalyst characterization

Table 4 presents the morphological properties of the synthesized solids. The specific surface area and the pore size distribution of the solid were obtained from nitrogen adsorption isotherm measurements, and prior to the measurements the samples were pre-treated at 100°C for 24 h. The specific surface area of Zn-N was 28 m^2/g, the pore volume was 5.1×10^{-2} cm^3/g, with an average pore radius of 23 nm. In the case of Zn-A, the specific surface area was 25 m^2/g, the pore volume was 5.4×10^{-2} cm^3/g, with an average pore radius of 23 nm.

Figure 1 shows the diffractograms for the Zn-N and Zn-A systems. The diffraction patterns observed are characteristic of layered crystalline solids, whose basal spacing (determined by Bragg's law) was of 9.73 Å for Zn-N, and 13.83 Å for Zn-A.

Figure 2 presents the DRIFT spectra of Zn-N and Zn-A. The DRIFT spectrum of Zn-N shows that in the

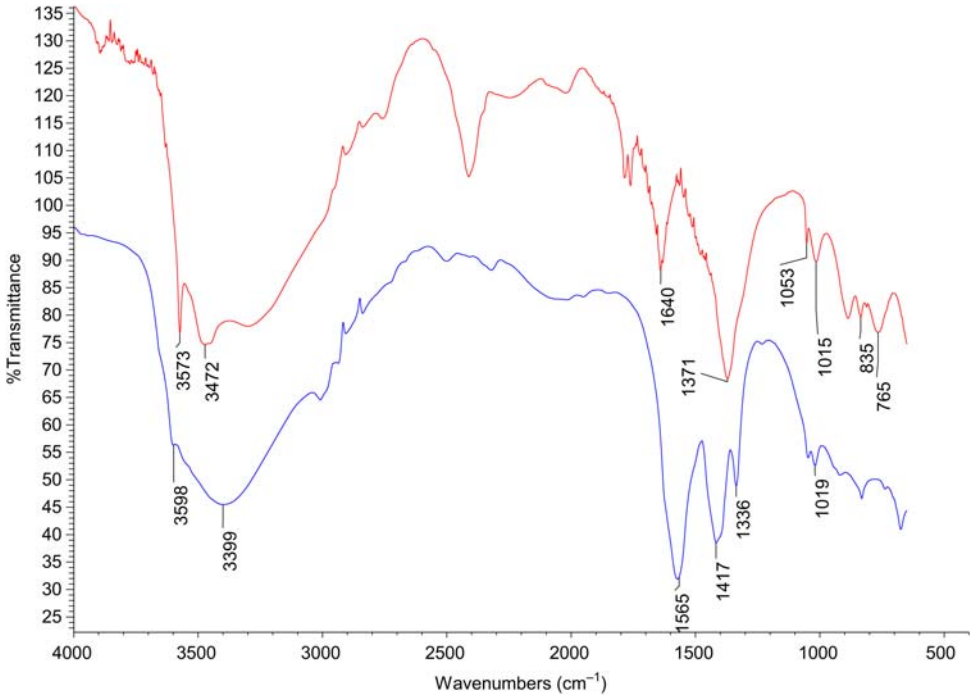

Figure 2. *DRIFT spectra of Zn-N and Zn-A catalysts.*

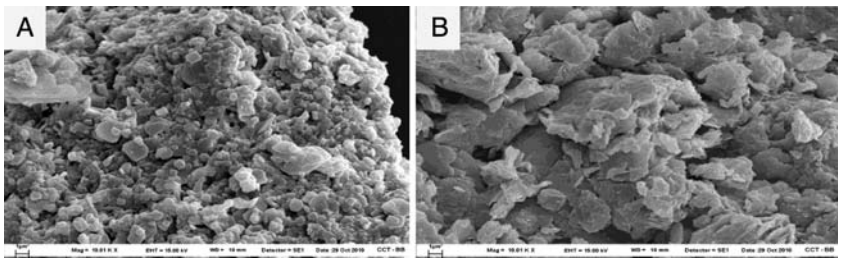

Figure 3. *SEM image of (A) Zn-N and (B) Zn-A.*

spectral range characteristic of nitrate stretching (1000–1500 cm^{-1}) the band located at 1371 cm^{-1} is assigned to the stretching mode of free nitrate ions. The other nitrate absorption bands are the weak bands located at 765 cm^{-1} (symmetric deformation) and 835 cm^{-1} (asymmetric deformation). The weak band at 1063 cm^{-1} is attributed to N–O stretching of free nitrate groups. The weak broad band at 1015 cm^{-1} is attributed to the O–H bending mode in the Zn–OH entities. The spectrum corresponding to the synthesized sample also showed a strong absorption band at 1635 cm^{-1} characteristic of the bending vibrations of the interlayer water molecules. In the spectral region of the OH group stretching vibrations (2900–3700 cm^{-1}), the bands originated by the presence of the hydroxyl layer, as well as hydrogen bonds from the hydroxyl layer, water molecules and nitrate groups can be observed. The band at the lower frequency is attributed to the OH groups implicated in hydrogen bonding, and the sharp band located at 3573 and 3576 cm^{-1} at the upper frequency limit relates to the free OH groups [18].

In the DRIFT spectrum of Zn-A shown in Figure 2, the stretching vibration bands are observed from 2900 to 3500 cm^{-1}. The strong band observed at 3673 cm^{-1} can be attributed to stretching vibrations of OH groups not involved in hydrogen bonding, and the broad band at 3450 cm^{-1} can be ascribed to OH groups involved in hydrogen bonding. The bands of symmetric and asymmetric stretching vibrations of interlayer acetate anions were observed at 2900 cm^{-1}. The sharp absorption bands at 1585 and 1391 cm^{-1} can be ascribed to the symmetric and asymmetric stretching vibrations of the carboxylic group from the acetate anion. The bands at 1338 and 1021 cm^{-1} are attributed to the asymmetric deformation of CH_3 groups and the bending vibrations of the OH group, respectively. The H_2O bending mode was expected to appear at 1600 cm^{-1}, but it was probably overlapped by the sharp and broad band produced by the asymmetric stretching of CO_2 [17].

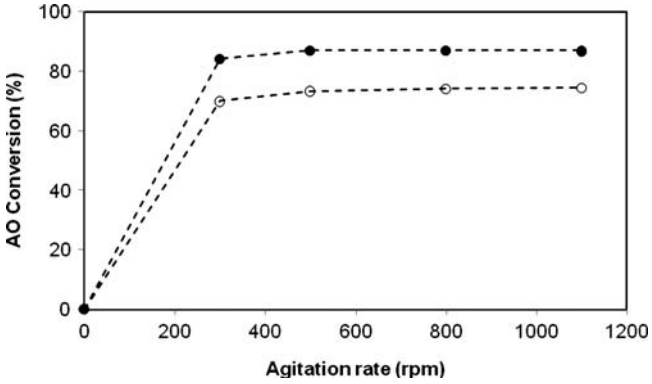

Figure 4. *OA conversion, at 140°C, 3% catalyst and 2 h of reaction. Reference: (filled circle) Zn-A, (open circle) Zn-N.*

Table 5. *Catalytic results for the 2^3 factorial and face-centered CCD.*

Temperature (°C)	Catalyst loading (% wt with respect to OA)	MOH:OA molar ratio (mol:mol)	AO conversion (%)
100	3	30	13.87
100	1	30	11.27
100	3	10	10.92
100	1	10	9.80
120	2	20	20.12
120	2	20	20.90
140	3	30	73.36
140	1	10	32.88
140	3	10	72.37
140	1	30	35.50
100	2	20	11.49
140	2	20	44.63
120	1	20	15.80
120	3	20	28.21
120	2	10	18.87
120	2	30	25.34

Table 6. *Analysis of variance for OA conversion response.*

Source	Sum of squares	Degrees of freedom	Mean square	*F*-Snedecor	*P*-value
A	4071.92	1	4071.92	13385.67	0.0055
B	873.85	1	873.85	2872.62	0.0119
C	21.03	1	21.03	69.12	0.0762
AA	168.30	1	168.30	553.25	0.0270
AB	677.67	1	677.67	2227.72	0.0135
AC	0.08	1	0.08	0.27	0.6951
BB	12.02	1	12.02	39.50	0.1005
BC	0.003	1	0.003	0.01	0.9390
CC	13.17	1	13.17	43.28	0.0960
Lack of fit	63.58	5	12.72	41.80	0.1153
Pure error	0.30	1	0.30		
Cor. total	6122.54	15			

Figures 3 and 4 show the SEM images of the synthesized solid catalysts. In the image corresponding to Zn-N (Figure 3), plate-like particles can be observed, whereas in that of Zn-A (Figure 4) the particles are more flake-like. In both images a uniform particle distribution is observed.

3.2 Catalytic tests

3.2.1 *Effect of the agitation rate*

Figure 4 presents the OA conversion for different agitation rates for the Zn-N and Zn-A catalysts at 3% concentrations, 140°C and at 2 h of reaction. It can be observed that conversion did not increase at agitation rates higher than 500 rpm, indicating that there is no external mass-transfer resistance.

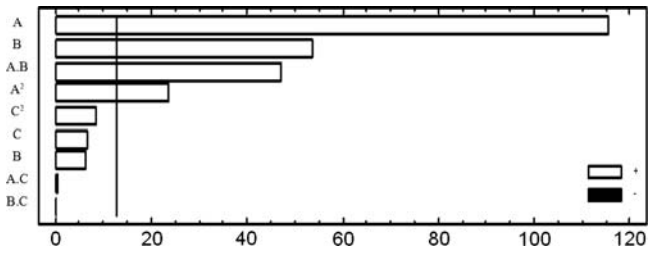

Figure 5. *Standardized pareto chart for the OA conversion response.*

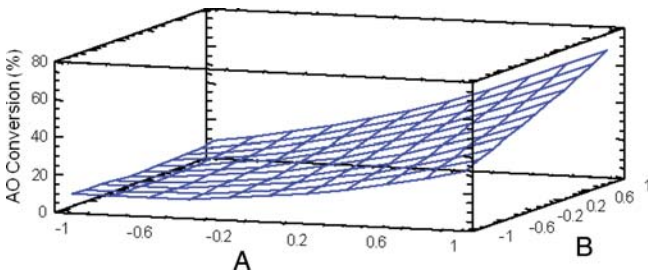

Figure 6. *Response surface for the effect of the reaction conditions (A: temperature, B: catalyst loading) on OA conversion (%), with C = 0 (MOH:OA molar ratio = 20).*

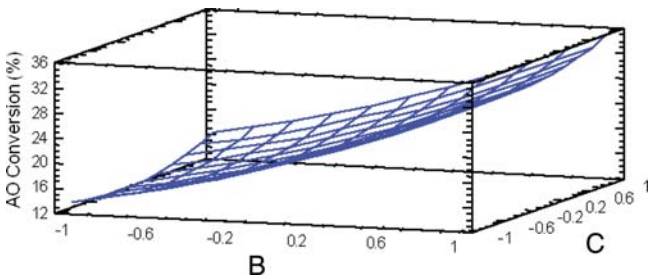

Figure 7. *Response surface for the effect of the reaction conditions (A: temperature, C: MOH:OA molar ratio) on OA conversion (%), with B = 0 (catalyst loading = 2%).*

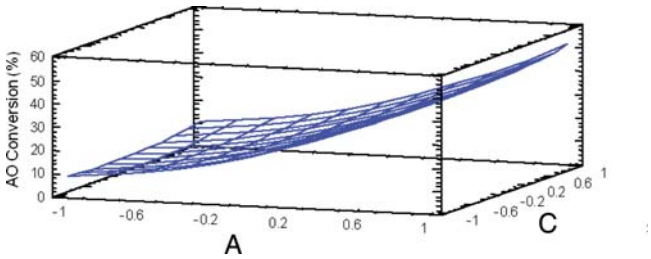

Figure 8. *Response surface for the effect of the reaction conditions (*B*: catalyst loading,* C*: MOH:OA molar ratio) on OA conversion (%), with* A = *0 (temperature = 120°C).*

3.2.2 *Analysis of the experimental design for Zn-N catalyst*

Table 5 shows the experimental catalytic results for the 2^3 factorial and face-centered CCD.

A first-order model was used to approximate the response obtained by the 2^3 design (with two additional points of the center for error estimation). The linear model generated a $R^2 = 0.93$. However, the lack of fit was significant ($P = 0.0014$). Therefore the first-order model was not an appropriate approximation for the response studied, and it was necessary to extend the design so that the application of a higher-order model was possible. Six experiments were added in order to obtain a face-centered CCD (Table 3). The quadratic model obtained from the fitted experimental data is presented in Equation (3). Table 6 shows the results from the analysis of variance for this model.

$$\text{OA conversion } (\%) = 20.08 + 20.18A + 9.35B + 1.45C + 7.99A^2 + 9.20AB - 0.10AC - 2.13B^2 - 0.02BC + 2.23C^2 \quad (3)$$

The fraction of variance explained by the model is 99.0% ($R^2 = 0.990$). The lack of fit was not significant ($P > 0.05$). Thus the quadratic model is adequate to represent the conversion data of OA.

The pareto chart (Figure 5) is presented to visualize the effect of the factors and interactions, where it can be observed that temperature, catalyst loading and their interactions were the most significant ones. Next in importance was the quadratic effect of the temperature factor. The rest of the terms were not significant.

The three-dimensional response surfaces were obtained by varying two factors within the experimental range, and keeping the third factor constant at the central point (Figures 6–8). It can be observed that the most marked effects are temperature (A), catalyst loading (B) and their interaction, as represented by the pareto chart. This interaction can be seen in Figure 6, where it is observed that at low values of the factor temperature ($A = -1$) the response does not vary markedly with the variation of the catalyst loading factor (B). However, as temperature increased, the influence of the catalyst loading becomes apparent. Likewise the effect of temperature on the

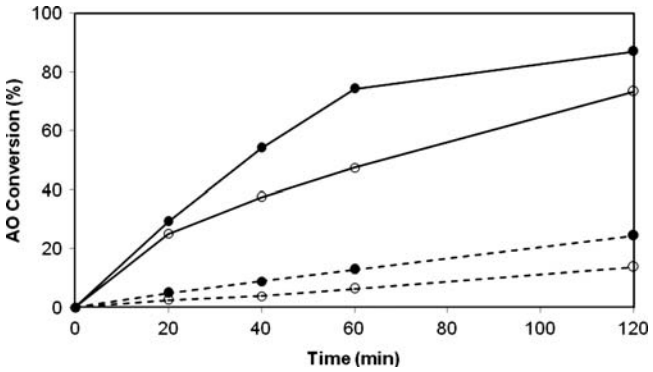

Figure 9. *Effect of temperature on the esterification of OA with MOH. Reaction conditions: 3% catalyst loading, OA:MOH molar ratio = 1:30. Reference: (filled circle) Zn-A, (open circle) Zn-N, (dashed line) 100°C, (continuous line) 140°C.*

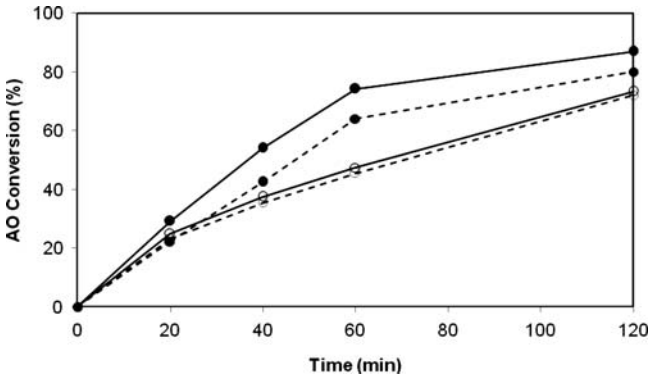

Figure 10. *Effect of the MOH:OA molar ration on the esterification of OA. Reaction conditions: 3% catalyst loading, temperature: 140°C. Reference: (filled circle) Zn-A, (open circle) Zn-N, (dashed line) OA:MOH = 1:10, (continuous line) OA:MOH = 1:30.*

response is more evident when the catalyst loading is high ($B = 1$). The non-significant effect of C can be observed in Figures 7 and 8. Likewise, the quadratic effect of factor A is shown by means of the curvature of the response surface in Figure 8.

Equation (4) presents the simplified model (without considering the terms that were not significant):

$$\text{OA conversion } (\%) = 21.54 + 20.18A + 9.35B + 10.03A^2 + 9.20AB \quad (4)$$

Within the range of operating conditions of the model, the highest conversion (optimum value) for Zn-N was observed at 140°C and 3% catalyst loading, generating a conversion predicted by the model of 70.3%, close to the experimental value of 73.4% for $A = 1$, $B = 1$ and $C = 1$, and 72.4% for $A = 1$, $B = 1$ and $C = -1$.

In order to validate the model, an additional experiment was carried out at 140°C, 2% catalyst loading and MOH:AO

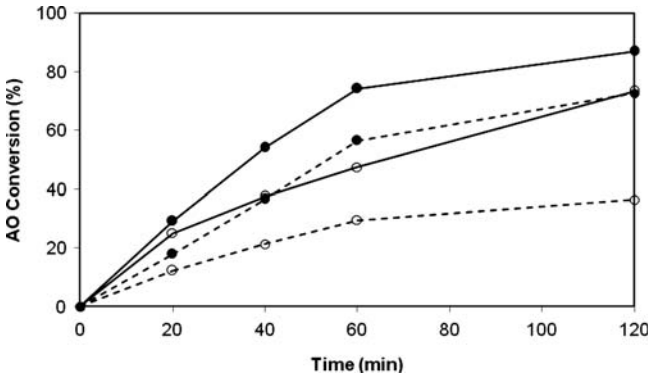

Figure 11. *Effect of the catalyst loading on the esterification of OA with MOH. Reaction conditions: temperature: 140°C, OA:MOH molar ratio = 1:30. Reference: (filled circle) Zn-A, (open circle) Zn-N, (dashed line) 1% catalyst loading, (continuous line) 3% catalyst loading.*

molar ratio of 30:1, corresponding to the point [1, 0, 1] of the coded variables. The experimental value of the OA conversion was 54.0%, close to the result predicted by the model presented in Equation (4) (51.8%), generating a relative error of 4%.

3.2.3 *Zn-A catalyst performance*

Figure 9 presents OA conversion as a function of reaction time for the catalyst Zn-A, compared with Zn-N at 100 and 140°C. The results showed that the catalytic activity of Zn-A is strongly affected by the change in temperature. Conversions of 24.4 and 87.0% were obtained for reaction temperatures of 100 and 140°C, respectively. This behavior was similar to that observed in Zn-N, in which conversions were 13.9 and 73.4% for 100 and 140°C, respectively.

The increase in temperature increases the kinetic constant of the reaction, as predicted by the Arrhenius equation, and thus reaction temperature should be as high as possible. On the other hand, using high temperatures implies high energy costs, which should be taken into account in the overall evaluation to select the operating conditions.

When comparing the results obtained for the solids, it is observed that the performance of Zn-A in the methyl esterification of OA is higher than that of Zn-N.

In the tests performed by varying the MOH:OA molar ratio, the results showed that the catalytic activity of Zn-A was slightly affected by the variation of the MOH:OA molar ratio (Figure 10). Conversions of 87.0 and 80.0% were obtained for MOH:OA molar ratios of 1:30 and 1:10, respectively, whereas when working with Zn-N the conversions obtained were 73.4 and 72.4% for 1:30 and 1:10, respectively, and therefore the effect of this variable on the catalyst performance was minimum.

It is interesting to point out that the use of an excess of MOH is not always adequate and has limitations, given that MOH recovery is expensive.

A series of tests were carried out to analyze the effect of the catalyst loading on the reaction, the results of which are shown in Figure 11. It can be observed that an increase in the catalyst

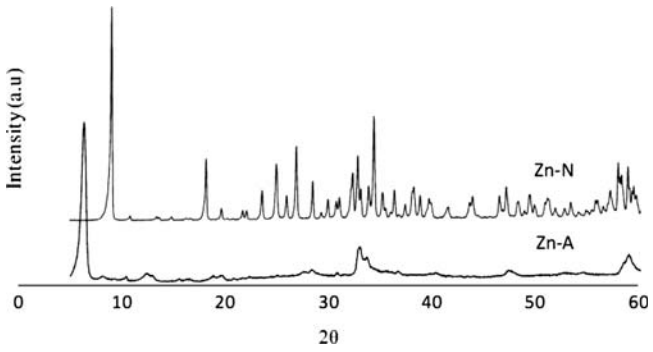

Figure 12. *DRX spectra of Zn-A and Zn-N used in esterification reaction.*

concentration had a lower effect on the catalytic activity of Zn-A than of Zn-N. For Zn-A, conversions of 87.0 and 72.7% were obtained for catalyst concentrations of 3 and 1%, respectively, whereas for Zn-N the conversions obtained were 73.4 and 35.5% for 3 and 1%, respectively. As mentioned above, there is no external mass-transfer resistance, and it could be assumed that neither is there internal, since the catalysts are fine powder. These differences could be attributed to the modification undergone by the solids, which will be discussed below.

3.2.4 *Analysis of the spent catalyst*

The catalysts used in reaction were recovered by washing in a tetrahydrofuran/MOH (50/50) solution, filtered and dried in oven at 50°C, and then characterized. Figure 12 shows the diffractogram for Zn-A and Zn-N after being used, where both solids present the same structure, different from the original one. The basal spacing was of 14.07 and 13.98 Å for spent Zn-A and Zn-N, respectively.

Figure 13 shows the DRIFT spectra of the spent solids, where the bands located at 2953, 2918 and 1849 cm^{-1} are attributed to the axial deformation vibrational modes of C–H in the aliphatic chain. The bands located at 1463 cm^{-1} correspond to the angular deformations of these ligands, and the bands at 1541 and 1397 cm^{-1} correspond to vibrations of the carboxylate ion. An intense band can be observed between 2900 and 3500 cm^{-1}, corresponding to the axial deformation of O–H groups. When compared with Figure 2, it can be observed for Zn-N that the signal corresponding to Zn–OH decreased markedly (1015 cm^{-1}) and the bands for C–H begin to appear. Regarding the signals of the nitrate ion, the signal at 830 cm^{-1} decreased and the rest of the signals overlapped with some present in the carbon chain of the OA: –C–H (CH_3) (at 1373 cm^{-1}), –$(CH_2)_n$-*cis*, (at 723 cm^{-1}).

For Zn-A, when compared with Figure 2, the signals corresponding to C–H intensified (2900 cm^{-1}), whereas the signals corresponding to the carboxylate group (1542, 1390 cm^{-1}) decreased slightly. For both catalysts, the signal corresponding to the O–H groups is similar, and lower than in the original samples (before use).

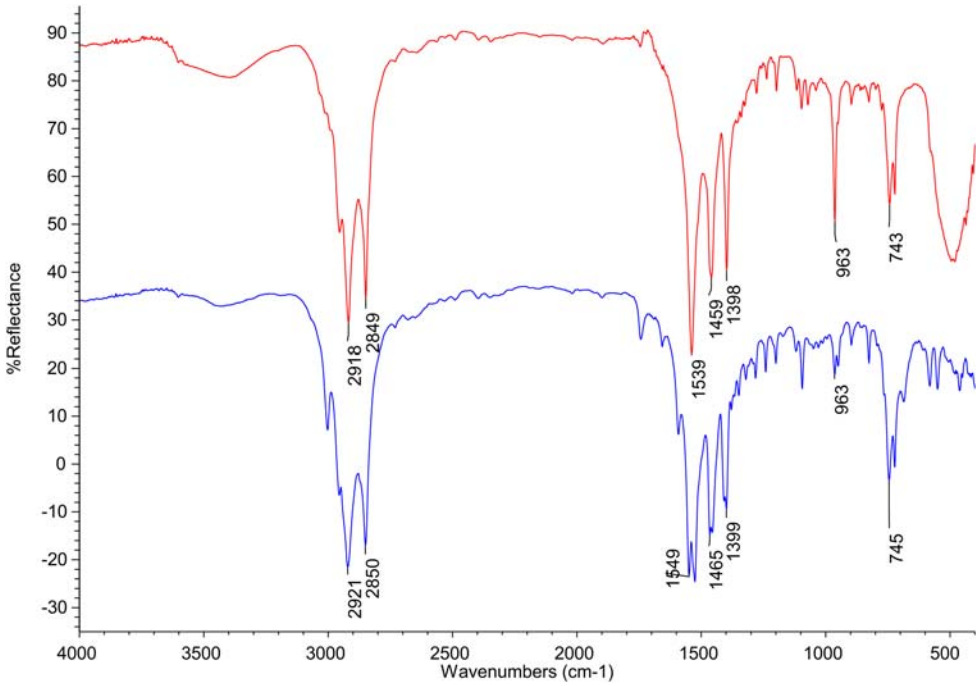

Figure 13. *DRIFT spectra of Zn-A and Zn-N catalysts used in esterification reaction.*

IR and XRD results indicate that the nitrate and acetate ions could have been replaced with the oleate ion in the layered material. Cordeiro *et al.* [9] reported that spent Zn-N presented a similar structure to that of the salt of esterified fatty acid (lauric acid), but it also matched with compounds obtained by the exchange of carboxylate anions within LDH of di- and trivalent cations. The results presented in this work show that Zn-A undergoes the same transformation, in spite of having a larger anion in its structure.

4 CONCLUSIONS

The layered solid Zn-A was seen to be more active than the salt Zn-N for the esterification of OA with MOH in the different reaction conditions studied. Conversions were 87.0 and 73.4% for the Zn-A sample and the solid Zn-N, respectively, when working at 140°C, with an OA:MOH molar ratio of 1:30 and a catalyst loading of 3% p/p.

The tests indicated that the catalytic activity of Zn-A is strongly affected by temperature, whereas the catalyst loading and molar ratio variables have a lesser effect on the performance of the solid in the reaction studied.

ACKNOWLEDGEMENTS

The authors thank Universidad Nacional del Sur and Consejo Nacional de Investigaciones Científicas y Técnicas for the financial support.

REFERENCES

[1] Sharma Y, Singh B, Upadhyay S. Advancements in development and characterization of biodiesel: a review. *Fuel* 2008;**87**:2355–73.

[2] Meher L, Sagar D, Naik S. Technical aspects of biodiesel production by transesterification—a review. *Energy Rev* 2006;**10**:248–68.

[3] Knothe G, Van Gerpen J, Krahl J. *The Biodiesel Handbook*, 1st edn. AOCS Press, 2004.

[4] Van Germen J. Biodiesel processing and production. *Fuel Process Technol* 2005;**86**:1097–107.

[5] Canakci M, Van Gerpen J. Biodiesel production from oils and fats with high free fatty acids. *Am Soc Agric Eng* 2001;**44**:1429–36.

[6] Marchetti J, Miguel V, Errazu A. Technol. Techno-economic study of different alternatives for biodiesel production. *Fuel Process* 2008;**89**;740–8.

[7] Choudary B, Kantam M, Reddy C, *et al.* Mg–Al–O–t-Bu hydrotalcite: a new and efficient heterogeneous catalyst for transesterification. *Mol Catal A* 2000;**159**;411–6.

[8] Antunes W, Veloso C, Henriques C. Transesterification of soybean oil with methanol catalyzed by basic solids. *Catal Today* 2008;**133–135**:548–54.

[9] Cordeiro C, Carabajal Arizaga G, Pereira Ramos L, *et al.* A new zinc hydroxide nitrate heterogeneous catalyst for the esterifcation of free fatty acids and the transesterifcation of vegetable oils. *Catal Commun* 2008;**9**:2140–3.

[10] Zieba A, Pacula A, Drelinkiewicz A. Transesterification of triglycerides with methanol catalysed by heterogeneous zinc hydroxy nitrate catalyst. Evaluation of variables affecting the activity and stability of catalyst. *Energy Fuels* 2010;**24**:634–45.

[11] Zieba A, Pacula A, Serwicka E, *et al.* Transesterification of triglycerides with methanol over thermally treated $Zn_5(OH)_8(NO_3)_2.2H_2O$ salt. *Fuel* 2010;**89**:1961–72.

[12] Auffredic J, Louer D. Etude thermodynamique de la décomposition thermique des hydroxynitrates de zinc. *J Solid State Chem* 1983;**46**:245–52.

[13] Poul L, Jouini N, Fievet F. Layered hydroxide metal acetates (metal = zinc, cobalt, and nickel): elaboration via hydrolysis in polyol medium and comparative study. *Chem Mater* 2000;**12**:3123–32.

[14] Hosono E, Fujihara S, Kimura T, *et al*. Growth of layered basic zinc acetate in methanolic solutions and its pyrolytic transformation into porous zinc oxide films. *J Colloid Interface Sci* 2004;**272**:391–8.

[15] Kandare E, Heossenlopp J. Hydroxy double salt anion exchange kinetics: effects of precursor structure and anion size. *J Phys Chem B* 2005;**109**:8469–75.

[16] Newman S, Jones W. Comparative study of some layered hydroxide salts containing exchangeable interlayer anions. *J Solid State Chem* 1999;**148**:26–40.

[17] Biswick T, Jones W, Pacula A, *et al*. Evidence for the formation of anhydrous zinc acetate and acetic anhydride during the thermal degradation of zinc hydroxy acetate, $Zn_5(OH)_8(CH_3CO_2).4H_2O$ to ZnO. *J Solid State Sciences* 2009;**11**:330–5.

[18] Chouillet C, Kraft J, Louis C, *et al*. Characterization of zinc hydroxynitrites by diffuse reflectance infrared spectroscopy-structural modifications during thermal treatment. *Spectrochim Acta Part A* 2004;**60**:505–11.